Signature estimation using dual near-field hydrophones: sensitivity to noise and a proposed hybrid methodology

Rob Telling and Sergio Grion, Shearwater GeoServices

SUMMARY

We examine the effect of noise on signature estimation via least-squares inversion of near-field data. We look at the case of solving for real and virtual notional sources using twice the standard number of hydrophones within the source array. This approach has the advantage of being parameter-free as it removes assumptions on the magnitude of the sea-surface ghost and its period, but we find it is more sensitive to the presence of noise. This is due to the greater distances from the points of measurement to the unknown virtual notional sources when compared with distance to the real notional sources. We present results on field data for a hybrid methodology that utilizes the parameter-free approach at high frequency and a standard ghost model at low-frequency. We show that this approach ensures a good representation of both the ghost and the bubble oscillation.

Introduction

Near-field hydrophone (NFH) measurements within a source array may be used to derive, on a shot-by-shot basis, directional far-field signatures and a set of corresponding operators to use for de-signature of seismic data. The technique relies on the concept of deriving notional sources which encompasses the interaction between individual source elements (Ziolkowski et al. 1982). Refinements to this approach include the introduction of a least squares inversion method, incorporating bubble motion (Hargreaves et al. 2015) and data-adaptive schemes to handle variable ghost and frequency-dependent sea-surface reflectivity (Hargreaves et al. 2016, Telling et al. 2018a). However, the simplistic linear model of ghost formation appears to be inadequate for large airgun arrays since some loss of coherent energy is observed in the ghost, due to cavitation (Telling et al. 2018b, Khodabandeloo and Landro 2018). This makes it attractive to remove the explicit parameterization of the interaction at the free-surface and to replace it with a direct estimate of the down-going wave-field obtained through additional pressure measurements (Parkes and Hatton 1987, Hampson 2017, Kryvohuz and Campman 2017).

We study the joint inversion for real and virtual (ghost) notionals. Specifically, we examine the sensitivity of the method to the presence of noise in the near-field recordings. Previous work (Telling et al. 2018b) showed that de-signature improves at ghost notch frequencies but performs slightly poorer at bubble frequencies. However, it was not clear whether this was attributable solely to a raised noise level arising from the experimental temporary rigging used for the second hydrophone, or if it was more specific to the inversion process itself. Error analysis on the inversion process using singular-value decomposition (Hargreaves et al. 2015) indicates that the number of hydrophones and their positioning is very important for signal-to-noise ratio, and that increased separation of measurements from the guns can lead to poorer resolution of spatial variation of the notional sources. In this work we use the concept of posterior standard deviation (see for example Tarantola 2005) to understand the response of the inversion process to random noise and propose a solution to the problem of noise sensitivity at low frequencies

Method

The approach we use to estimate signatures from near-field hydrophone data relies on the established concept of solving for notional sources (Ziolkowski et al. 1982) within the framework of a least squares inversion (Hargreaves et al. 2015). In the frequency domain, the forward linear problem is given by:

$$\mathbf{d} = \mathbf{G}\mathbf{m} \qquad (1)$$

where **d** is a vector corresponding to the observed pressure data at each hydrophone position, **m** is a vector corresponding to the notional sources. **G** is a matrix operator which describes the propagation of acoustic energy from each source element to each hydrophone. Matrix elements are comprised of a geometric scaling term $1/r$ and a phase shift based on the delay time $\exp(-i\omega r/c)$ where r is the distance from a given source element to a given hydrophone and c the sound speed in water. The time-dependence of r due to relative motion of bubble and hydrophone is handled in between inverse and forward Fourier transforms. For simplicity, in the error analysis that follows we assume a static geometry. In the standard approach, we solve for notional sources at the real source element positions and **G** includes terms for the direct arrivals from source to hydrophone and their ghost reflected at the sea-surface, parametrized by a frequency varying reflection coefficient and delay path. In the parameter-free approach, we solve for real and virtual notional sources, with just the direct arrival terms considered. The posterior covariance of **G** in each case is given by (Tarantola 2005):

$$\tilde{\mathbf{C}}_{\mathbf{m}} = \left(\mathbf{G}^{*}\mathbf{C}_{\mathbf{d}}^{-1}\mathbf{G} + \mathbf{C}_{\mathbf{m}}^{-1}\right)^{-1} \qquad (2)$$

where the prior covariance matrices for the observed data, $\mathbf{C}_{\mathrm{d}} = \sigma_d^2\mathbf{I}$, and for the model, $\mathbf{C}_{\mathrm{m}} = \sigma_m^2\mathbf{I}$, are assumed to be diagonal and where σ_d and σ_m are their respective standard deviations, **I** is the identify matrix and the * denotes complex conjugate transpose. The posterior standard deviation of the model, $\tilde{\sigma}_m$ is then the square-root of the diagonal of the resulting covariance matrix.

Set-up

The geometry of source elements and hydrophones within the two-string array, used for the analysis and in the field trial of Telling et al. (2018b), is shown in Figure 1. We derive $\tilde{\sigma}_m$ for each notional signature (real or virtual). Note that while the virtual sources are mirrored above the sea-surface, the NFH cannot be in mirror positions. In our setup we have NFH at the standard 1m from source elements and a second set of NFH co-located within the horizontal plane but shallower by 2m.

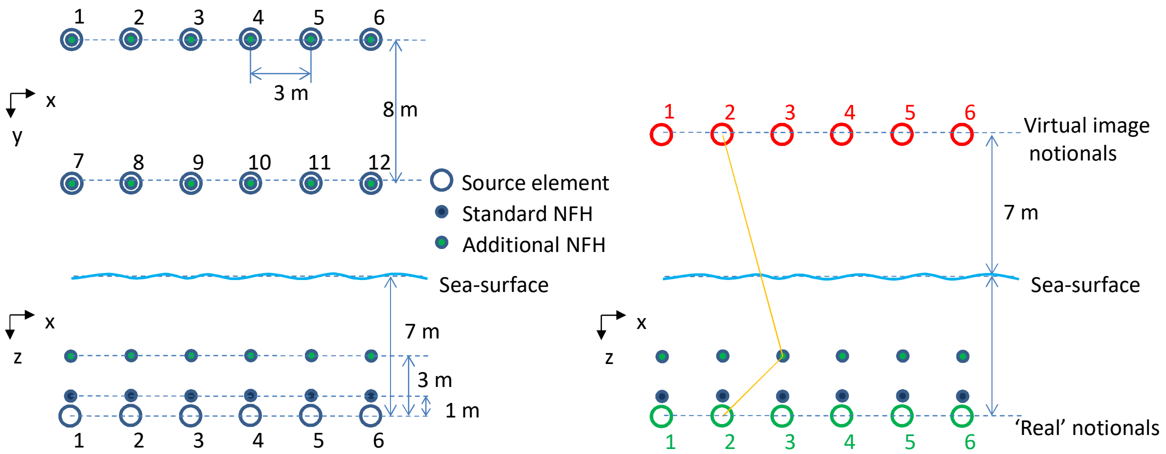

Figure 1 *Left: Schematic of array geometry in plan (top left) and side elevation (bottom left) showing source element and hydrophone locations and right: the positions of real and virtual notional sources in mirrored positions. The orange construction lines illustrate the asymmetry in distances for a particular hydrophone and real/virtual source combination.*

Figure 2 (left) shows a typical signal measured at a NFH during a bubble test plotted as a spectrogram showing the initial broadband burst of energy, followed by a decaying monotone at the fundamental bubble frequency of around 8 Hz, and a corresponding noise record (Figure 2, centre). Before processing, the low frequency ambient noise is around 20 dB less than the signal. For our qualitative analysis of the posterior standard deviation we assume priors $\sigma_d = 0.01$ at 0 Hz, reducing with frequency according to the trend observed in Figure 2 (centre), and $\sigma_m = 1.0$. The prior σ_d used is shown in Figure 2 (right).

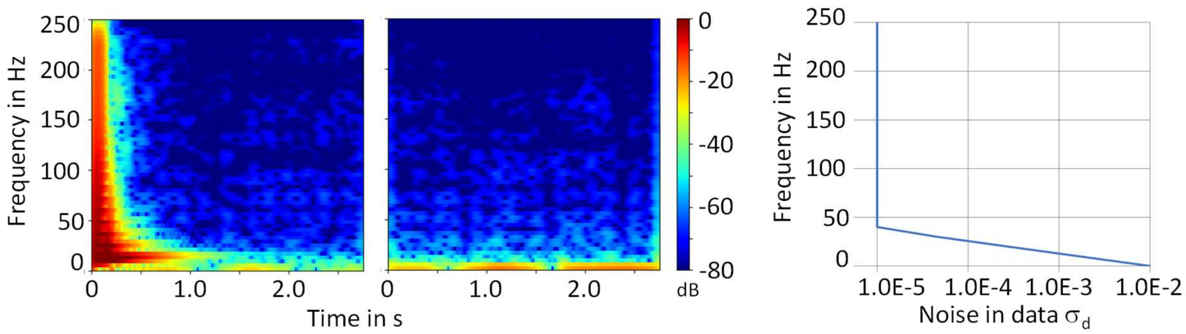

Figure 2 *Example spectrogram of recorded data at a NFH showing signal plus noise (left) and noise (centre), together with the extracted prior noise model as a function of frequency (right).*

We denote the operator with assumed free-surface and ghost model as $\mathbf{G_{FS}}$ and the operator with no free-surface assumption (i.e. that solves for separated real and virtual notional sources) as $\mathbf{G}$ and examine three inversion cases of interest *I1-I3* (see Table 1) with different number of hydrophones N_H, number of and number of virtual sources N_{SV}. The number of real sources N_{SR} is 12 for all three cases. *I1* and *I3* are of principal interest here, corresponding to the baseline and test scenarios. *I2* is the over-determined standard case.

Inversion type	Operator	NFH number	Virtual notionals
I1	$\mathbf{G}_{\mathbf{FS}}$	12	0
I2	$\mathbf{G}_{\mathbf{FS}}$	24	0
I3	$\mathbf{G}$	24	12

Table 1*: Experimental inversion types used for standard deviation calculations and de-signature tests*

Results

Figure 3 shows the posterior standard deviation, $\tilde{\boldsymbol{\sigma}}_{\boldsymbol{m}}$ as a function of frequency (0-125 Hz) for each derived ('real') notional in the first string of the array for cases *I1* and *I2* (standard inversions with differing numbers of hydrophones). For the assumed noise model there is a small reduction in uncertainty using the additional measurements, not visible at the scale of these figures. Figure 4 shows the same analysis applied to case *I3*, where the additional measurements are used to solve directly for both real and virtual notional sources, showing higher $\tilde{\boldsymbol{\sigma}}_{\boldsymbol{m}}$ for the virtual notional sources. The result on the virtual notional sources shows a significantly higher sensitivity to noise at low frequencies suggesting that inversion would be problematic. The sea-surface interaction is well-characterized at low frequency by a simple ghost model and therefore we propose a hybrid approach to overcome this issue, where the standard inversion *I2* is used for low frequencies and *I3* is used for high frequencies.

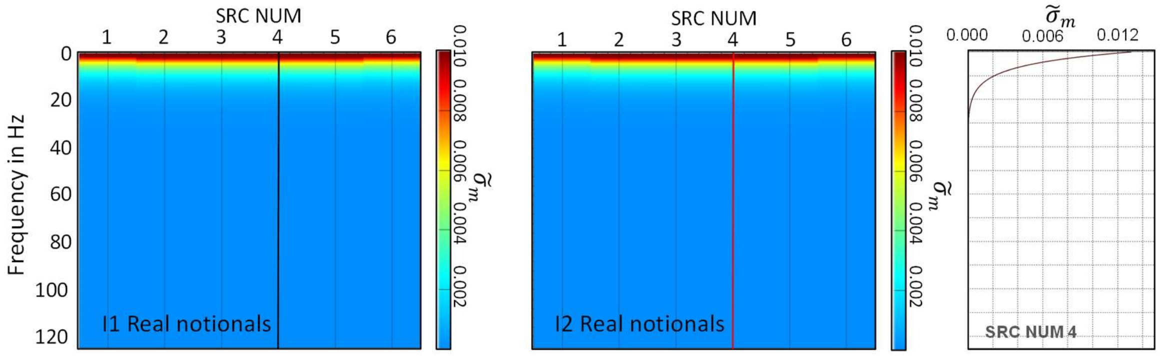

Figure 3 *$\tilde{\sigma}_m$ as a function of frequency plotted for real notional sources 1-6 on a colour scale and for notional #4 as a line plot for case I1 (N_H = 12, N_{SR} = 12) (left) and case I2 (N_H = 12, N_{SR} = 24) (right).*

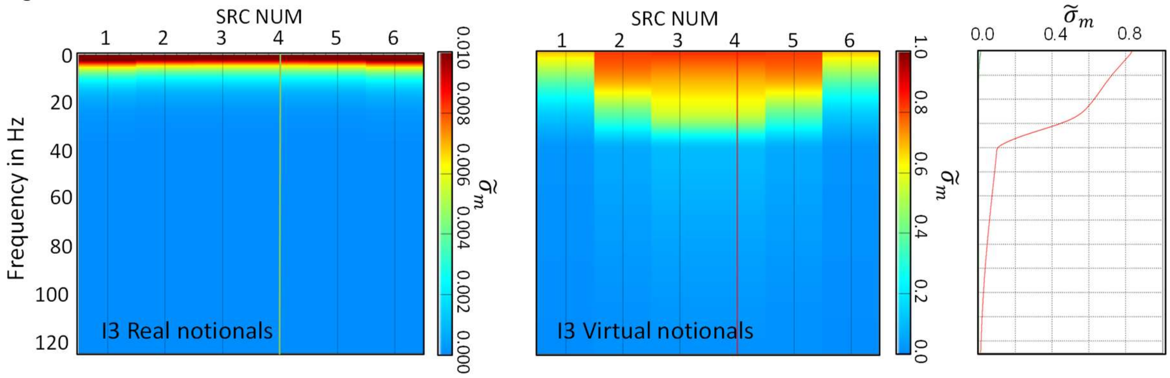

Figure 4 *$\tilde{\sigma}_m$ as a function of frequency for the dual hydrophone inversion, case I3 (N_H = 12, N_{SR} = 12, N_{SV} = 12) plotted for real notional sources 1-6 (left) and corresponding virtual notional sources 1-6 (right) on a colour scale and also with the real notional #4, and virtual notional #4 as line plots.*

The estimated far-field signatures derived for each inversion *I1-I3* are shown in Figure 5, together with the corresponding spectra of seismic data after de-signature. For *I1* and *I2* the frequency-varying reflectivity parameter was optimized via the proxy of a 4 m significant-wave-height term, which leads to comparable ghost amplitude as for the case of *I3*. Basic swell noise attenuation was applied to the NFH data prior to inversion. Note the problematic estimation of the bubble oscillation for case *I3* (red curve Figure 5, centre), which leads to mishandled low frequency in the seismic data after de-signature (red curve, Figure 5, right) and the improved hybrid result (green). The transition frequency for the hybrid method was chosen to be at 20 Hz.

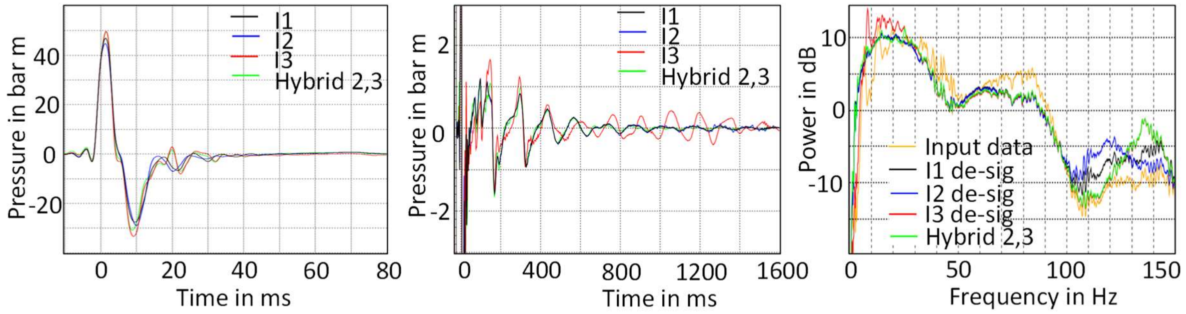

Figure 5 *Far-field signatures at normal take-off angle cropped to show main pulse and ghost (left) and, on a different scale, the subsequent bubble oscillations (centre). On the right are the spectra for the seismic data before and after de-signature using signatures derived via the different inversion cases I1-I3 and the hybrid of I2 and I3.*

Discussion

The sensitivity analysis of the standard and dual-NFH inversions gives us insight into the effect of noise on the quality of estimated signatures. We see a general tendency for greater sensitivity to noise at low frequency, and that this is more significant for the parameter-free dual NFH inversion than for the standard approach. Sensitivity is lower when NFHs are placed close to sources, but additional hydrophones cannot be placed closer to the virtual sources for practical reasons, including rigging, avoidance of direct interference with the sea surface and the presence of a higher level of swell noise at shallow depths. The greater sensitivity to noise, coupled with the higher level of noise at low frequencies, helps to explain the poorer estimation of the low frequency part of the total far-field signature for the parameter-free inversion compared to the standard inversion approach. However, we see promise in the results for a hybrid methodology that capitalizes on the advantages of the parameter-free approach at high frequency (> 20 Hz) and relies on the more robust standard inversion (with ghost model) at low-frequency, where the ghost model is known with better precision. This makes best use of the information from the additional hydrophones and ensures a good representation of ghost and of bubble oscillation, both important for accurate de-signature.

References

Hampson, G. [2017]. Notional ghosts. *86th Annual SEG Meeting,* Expanded Abstracts, 111-115.

Hargreaves, N., Grion, S. and Telling, R. [2015]. Estimation of air-gun array signatures from near-gun measurements - least-squares inversion, bubble motion and error analysis. *85th SEG Meeting,* Expanded Abstracts, 149-153.

Khodabandeloo, B and Landro M. [2018]. Acoustically induced cavity cloud generated b y air-gun arrays – comparing video recordings and acoustic data to modeling. *J. Acoust. Soc. Am.* **143** (6) 3383-3393.

Kryvohuz, M. and Campman, X. [2017]. Source-side up-down wavefield separation using dual NFHs, *79th EAGE Conference and Exhibition, Extended Abstracts*.

Parkes, G. and Hatton, L. [1986]. The Marine Seismic Souce. D. Reidel, Dordrecht.

Tarantola, A. [2005]. Inverse problem theory, SIAM.

Telling, R., Light, R., Grion, S., Denny, S. and Williams, R. G. [2018a]. Signature Estimation and Drop-Out Implications for a Triple Source Marine Seismic Survey. *80th EAGE Conference and Exhibition, Extended Abstracts*.

Telling, R., Grion, S., Denny, S. and Williams, R. G. [2018b]. Marine source signature estimation with dual near-field hydrophones. *86th Annual SEG Meeting, Expanded Abstracts,* 4070-4074.

Ziolkowski, A., Parkes, G., Hatton, L. and Haugland T. [1982]. The signature of an air gun array: Computation from near-field measurements including interactions. *Geophysics,* **47** (10), 1413-1421